Check for updates

Heterogeneous water oxidation photocatalysis based on periodic mesoporous organosilica immobilizing a tris(2,2′-bipyridine)ruthenium sensitizer†

Minoru Waki, [ID] * Soichi Shirai, [ID] Ken-ichi Yamanaka, [ID] Yoshifumi Maegawa [ID] and Shinji Inagaki [ID]

A periodic mesoporous organosilica (PMO) containing 2,2′-bipyridine groups (BPy-PMO) has been shown to possess a unique pore wall structure in which the 2,2′-bipyridine groups are densely and regularly packed. The surface 2,2′-bipyridine groups can function as chelating ligands for the formation of metal complexes, thus generating molecularly-defined catalytic sites that are exposed on the surface of the material. We here report the construction of a heterogeneous water oxidation photocatalyst by immobilizing several types of tris(2,2′-bipyridine)ruthenium complexes on BPy-PMO where they function as photosensitizers in conjunction with iridium oxide as a catalyst. The Ru complexes produced on BPy-PMO in this work were composed of three bipyridine ligands, including the BPy in the PMO framework and two X_2bpy, denoted herein as Ru(X)-BPy-PMO where X is H (2,2′-bipyridine), Me (4,4′-dimethyl-2,2′-bipyridine), *t*-Bu(4,4′-di-*tert*-butyl-2,2′-bipyridine) or CO_2Me (4,4′-dimethoxycarbonyl-2,2′-bipyridine). Efficient photocatalytic water oxidation was achieved by tuning the photochemical properties of the Ru complexes on the BPy-PMO through the incorporation of electron-donating or electron-withdrawing functionalities. The reaction turnover number based on the amount of the Ru complex was improved to 20, which is higher than values previously obtained from PMO systems acting as water oxidation photocatalysts.

Introduction

Over the past several decades, global energy demands have been primarily met by the combustion of fossil fuels including natural gas, oil and coal.[1] The use of these carbon-based energy sources has, in turn, led to environmental issues such as the depletion of petroleum resources, air pollution, and global warming. Thus, it is crucial to develop clean and sustainable energy sources that have the potential to mitigate global environmental problems.[2]

Artificial photosynthesis can provide clean energy from water and carbon dioxide under visible light irradiation.[3] Consequently, much attention has been focused on water oxidation as a means of generating electrons in artificial photosynthesis systems, and tris(2,2′-bipyridine)ruthenium $Ru(bpy)_3Cl_2$ is well known as a useful photosensitizer for visible light water oxidation.[4] The combination of a photosensitizer such as this with colloidal metal oxides, including RuO_2 or IrO_2, can effectively generate oxygen from water in a buffer solution

Toyota Central R&D Labs., Inc., Nagakute, Aichi 480-1192, Japan. E-mail: mwaki@ mosk.tytlabs.co.jp

† Electronic supplementary information (ESI) available: Fig. S1–S16 showing XRD patterns, nitrogen adsorption/desorption isotherms, UV/vis absorption and phosphorescence spectra, TEM and XAFS results. See DOI: 10.1039/d0ra00895h

including a sacrificial oxidant in response to photoirradiation.[5] The reaction mechanisms in these photocatalysis systems have been widely studied, and $Ru(bpy)_3Cl_2$ has been found to effectively absorb visible light based on metal-to-ligand-charge transfer (MLCT) with a long lifetime. In this process, the excited state is oxidized to $Ru(bpy)_3^{3+}$ by a sacrificial electron acceptor such as $S_2O_8^{2-}$.[6] This species functions as a sensitizer to produce oxygen from water over IrO_2. It should also be noted that the $Ru(bpy)_3^{3+}$ can rapidly decompose, which is kinetically competitive with the water oxidation reaction.[7] To date, the majority of photocatalysis systems have been heterogeneous, based on absorbing a transition metal complex dye sensitizer and a colloidal metal oxide catalyst on a support comprising TiO_2 and silica.[6] The incorporation and dispersion of the metal complex photosensitizer within the support material is vital to fabricating integrated photoreaction systems that mimic photosynthesis. As an example, a Ru polypyridine complex photosensitizer fixed on a solid support material can be tuned with regard to its photochemical properties and redox potential to match the catalyst or electron donor/acceptor, so as to promote an energy transfer and electron cascade.

Mesoporous materials have been employed to immobilize the catalyst and photosensitizer, since these substances exhibit

Paper

useful structural features such as large pores that provide a scaffold for photochemical reactions. Periodic mesoporous organosilica (PMO) is a unique solid support for catalysis because of its high stability (resulting from a covalent framework structure), large pore diameters (2–30 nm) that allow the facile diffusion of molecules, and its capacity to incorporate functional organic groups within the pore walls.[8,9] Previously, our group has constructed a water oxidation photocatalysis system based on a PMO in which acridone (Acd) groups are incorporated in a framework on which $Ru(bpy)_3^{2+}$ complexes are grafted as the photosensitizer and IrO_2 particles are deposited as the catalyst.[10] This Acd–PMO absorbs visible light and transfers the excitation energy to the $Ru(bpy)_3^{2+}$ grafted onto its surfaces. The excited state of the Ru complex is oxidatively quenched by a sacrificial oxidant to form Ru^{3+} species that extract electrons from the IrO_2 to oxidize water for oxygen production. However, the grafting of photosensitizers inhibits molecular diffusion through the pores, such that the ability of the Ru photosensitizer to promote water oxidation is reduced. In other work, PMOs containing a silylated tris(2,2′-bipyridine) ruthenium complex within their pore walls were newly synthesized and applied to water oxidation photocatalysis combined with IrO_2.[11] The Ru complex embedded in the pore walls served as a photosensitizer that promoted oxygen evolution via photocatalysis with an excellent quantum yield (17%). However, the turnover number (TON_{Ru}) based on the quantity of the Ru complex was still low because a large proportion of the photosensitizers was contained in the pore walls and so was not available for the reaction.

Recently, we reported that a PMO containing 2,2′-bipyridine (BPy-PMO) exhibited a unique pore wall structure in which 2,2′-bipyridine groups were densely and regularly packed and also exposed on the surfaces.[12] These surface bipyridine groups functioned as chelating ligands for the formation of metal complexes on the pore walls, such that isolated, well accessible catalytic sites were constructed in the mesopores. The immobilized metal complexes were present solely at the surface of the material and thus could be utilized to promote heterogeneous reactions. In previous work, the $Ru(bpy)_3^{2+}$ complex was synthesized directly on the surface bipyridine groups of the BPy-PMO, and applied as a photosensitizer for heterogeneous CO_2 reduction via photocatalysis.[13] Thus, a Ru complex supported on BPy-PMO is a good candidate for use as a heterogeneous photosensitizer catalyst to promote water oxidation, because of the structural features and unique solid ligand properties of this material.

Herein, we report the photocatalysis of water oxidation using several different types of Ru tris(bipyridine) complexes immobilized on BPy-PMO, in conjunction with iridium oxide under visible light in the presence of a sacrificial oxidant. Efficient photocatalysis was achieved by tuning the photochemical properties of the Ru complexes on the BPy-PMO through the incorporation of substituents on the bpy ligands. Each Ru complex on the solid surfaces of this catalyst has three ligands; a BPy group in the PMO framework and two X_2bpy ligands. The latter are denoted herein as Ru(X)-BPy-PMO, where X is H (2,2′-bipyridine), Me (4,4′-dimethyl-2,2′-bipyridine = dmbpy), t-Bu(4,4′-di-tert-butyl-2,2′-bipyridine = dtbbpy) or CO_2Me (4,4′-dimethoxycarbonyl-2,2′-bipyridine = dmcbpy) (Scheme 1). Ru(CO_2Me)-BPy-PMO, which incorporates an electron withdrawing group, exhibits a high TON_{Ru} during photocatalytic water oxidation. Quantum chemical calculations and photochemical studies suggest that the photo-induced electron transfer associated with the photocatalytic water oxidation process occurs on the surface of the Ru(CO_2Me)-BPy-PMO when used with IrO_2 in the presence of a sacrificial oxidant.

Experimental

Synthesis

The dmbpy, dtbbpy, and dmcbpy were commercially available and were used without further purification. Ru complex precursors, $[Ru(dmbpy)_2(dmso)Cl]Cl$,[14] $Ru(dtbbpy)_2Cl_2$,[15] and $Ru(dmcbpy)_2Cl_2$,[16] were prepared according to the literature published previously.

Ru(Me)-BPy-PMO. To an ethanol (12 mL) solution of $[Ru(dmbpy)_2(dmso)Cl]Cl$ (29 mg, 0.047 mmol; dmso = dimethyl sulfoxide) was added BPy-PMO (0.075 g) under an Ar atmosphere. The mixture was kept under continuous stirring and refluxed at 90 °C for 20 h. The resulting powder was recovered by filtration, then washed with $CHCl_3$ and ethanol to remove any unreacted $[Ru(dmbpy)_2(dmso)Cl]Cl$, affording Ru(Me)-BPy-PMO.

Ru(t-Bu)-BPy-PMO. To an ethanol (12 mL) solution of $Ru(dtbbpy)_2Cl_2$ (0.12 g, 0.15 mmol) was added BPy-PMO (0.075 g) under an Ar atmosphere. The mixture was kept under continuous stirring and refluxed at 90 °C for 20 h. The resulting powder was recovered by filtration, then washed with $CHCl_3$ and ethanol to remove any unreacted $Ru(dtbbpy)_2Cl_2$, affording Ru(t-Bu)-BPy-PMO.

Ru(CO_2Me)-BPy-PMO. To an ethanol (8 mL) and H_2O (8 mL) solution of $Ru(dmcbpy)_2Cl_2$ (29 mg, 0.039 mmol) was added BPy-PMO (0.10 g) under an Ar atmosphere. The mixture was kept under continuous stirring and refluxed at 90 °C for 20 h. The resulting powder was recovered by filtration, then washed with $CHCl_3$ and ethanol to remove any unreacted $Ru(dmcbpy)_2Cl_2$, affording Ru(CO_2Me)-BPy-PMO.

Analyses

XAFS. X-ray absorption fine structure (XAFS) spectra at the Ru K-edge were acquired in the transmission mode at 298 K on
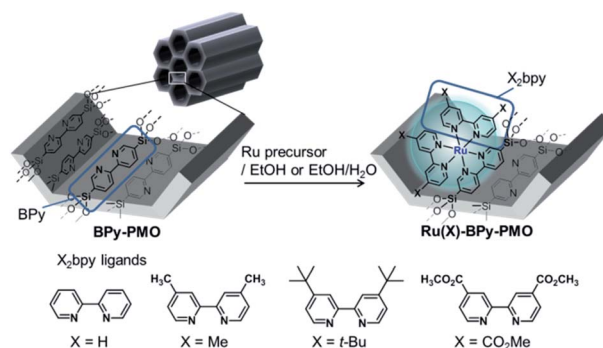
Scheme 1 Preparation of Ru complexes supported on BPy-PMO.

the BL14B2 station at the SPring-8 facility with the approval of the Japan Synchrotron Research Institute (JASRI) (proposal Numbers 2014B1899 and 2016B1617). The stored current and beam energy in the storage ring were 100 mA and 8 GeV, respectively. X-rays from the storage ring were mono-chromatized by channel-cut Si(311) crystals. Ionizing chambers filled with pure Ar and Kr were used to monitor the incident and transmitted X-rays, respectively. Extended X-ray absorption fine structure (EXAFS) data were analysed with the Athena and Artemis software packages, using the IFEFFIT suite of programs. The k^3-weighted Ru K-edge EXAFS oscillations (30–160 nm^{-1}) were processed by Fourier transform into R-space to allow curve-fitting. The fitting parameters were the coordination number (CN), interatomic distance (R), Debye–Waller factor (σ^2) and edge energy correction (ΔE_0). Phase shifts and backscattering amplitudes were calculated with the FEFF6 code.

Photocatalytic reactions. A quantity of the powdered Ru-BPy-PMO (10 mg) was dispersed in a hydrolysed solution (50 mL) of IrCl$_3$ (1.2×10^{-4} M) in the presence of a sacrificial oxidant, Na$_2$S$_2$O$_8$ (3.1×10^{-2} M). The suspension was subsequently introduced into a vessel connected to a glass-enclosed gas-circulation and evacuation system. The vessel was degassed under vacuum and then purged with gaseous Ar four times. Finally, Ar was introduced until an internal pressure reached 620 Torr. Visible light at wavelengths above 385 nm was supplied by an 800 mW xenon lamp. Aliquots of the gas phase in the vessel were periodically sampled and analysed using a gas chromatograph (SHIMADZU GC-8A) coupled with a thermal conductivity detector (TCD) and a molecular sieve 5 Å column (mesh 60/80, 2 m, Ø3 mm i.d.). It carried out at 60 °C of detection temperature in an argon carrier gas. TONs based on Ru amount were estimated according to an equation of TON$_{Ru}$ = (O$_2$ amount evolved [mol])/(Ru amount used [mol]).

Computations

Ab initio quantum chemical calculations were carried out for [Ru(sibpy)(X$_2$bpy)$_2$]$^{2+}$ model complexes, where sibpy is 5,5′-{Si(OH)$_3$}$_2$-2,2′-bpy. This moiety approximates the bpy ligand of BPy-PMO (Scheme S1†). The molecular structures of [Ru(sibpy)(X$_2$bpy)$_2$]$^{2+}$ were optimized using the density function theory (DFT) method and the molecular orbitals at the optimized geometries were analysed. The model is denoted herein as RuBP(X) (X = H, Me, t-Bu or CO$_2$Me). The first triplet (T$_1$) states were additionally calculated to examine the distribution of the excited electron. The solvent effect of water was also incorporated into the calculations. Details of the calculations are presented in the ESI.†

Results & discussion

Characterization of the Ru(X)-BPy-PMO specimens

The Ru(X)-BPy-PMO materials were synthesized *via* the post-coordination of the complexes on the BPy-PMO surface. Ru(H)-BPy-PMO and Ru(Me)-BPy-PMO were obtained using *cis*-[Ru(bpy)$_2$(dmso)Cl]Cl and *cis*-[Ru(dmbpy)$_2$(dmso)Cl]Cl, respectively, as precursors, employing a previously reported method.[13]

Table 1 Textural properties of Ru(X)-BPy-PMOs

Ru(X)-BPy-PMO	Ru^a/μmol g^{-1}	S_{BET}/m^2 g^{-1}	D_{DFT}/nm	V_{t-plot}/cm^3 g^{-1}
X = H	91	730	3.54	0.409
X = Me	67	719	3.54	0.403
X = t-Bu	89	718	3.54	0.384
X = CO$_2$Me	58	665	4.78	0.383

^{a} Determined by ICP.

Use of these Ru-dmso complex precursors was an efficient means of introducing the Ru complexes into the PMO, due to the high solubility of these species in the reaction solvents. Ru(t-Bu)-BPy-PMO and Ru(CO$_2$Me)-BPy-PMO were prepared using *cis*-Ru(dtbbpy)$_2$Cl$_2$·2H$_2$O and *cis*-Ru(dmcbpy)$_2$Cl$_2$·2H$_2$O, respectively, as precursors, both of which are readily soluble in EtOH or EtOH/water. Methoxycarbonyl group of Ru(CO$_2$Me)-BPy-PMO would be tolerant of ester exchange or hydrolysis under the complex formation condition, as with the preparation of homogeneous Ru complex, [Ru(dmcbpy)$_2$(bpy)]$^{2+}$. The Ru complex loading amounts were estimated from inductively coupled plasma (ICP) analyses. As shown in Table 1, the Ru complexes were loaded at concentrations of 58–91 μmol g^{-1}, equivalent to the use of 4–6% of the available surface BPy units.

The periodic mesopore structures of the Ru(X)-BPy-PMOs were found to be completely retained during metal complex formation in conjunction with the refluxing of EtOH suspensions. This was confirmed by X-ray diffraction (XRD) and nitrogen adsorption/desorption isotherms (Fig. 1 and S1–S3†). The XRD patterns acquired from the Ru(CO$_2$Me)-BPy-PMO
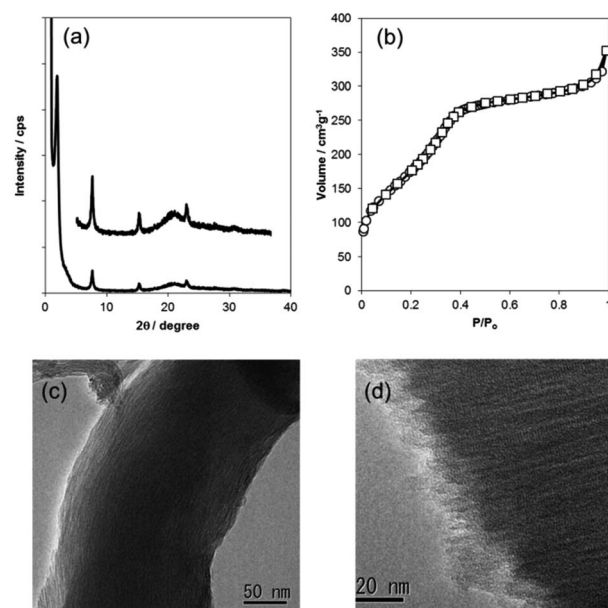

Fig. 1 (a) The XRD pattern and (b) the nitrogen adsorption/desorption isotherm obtained from the Ru(CO$_2$Me)-BPy-PMO. The inset to (a) shows a magnified scale in the medium angle range. (c) and (d) TEM images of the Ru(CO$_2$Me)-BPy-PMO.

Table 2 Curve-fitting results from Fourier transforms of Ru K-edge EXAFS data for the Ru(X)-BPy-PMOs

Ru(X)-BPy-PMO	CN	Distance/Å	ΔE_0/eV	σ^2/nm^2
X = H	6.14 ± 1.87	2.07 ± 0.012	−4.13 ± 4.13	0.0025 ± 0.0014
X = Me	5.91 ± 2.52	2.08 ± 0.014	−2.33 ± 0.01	0.0028 ± 0.0019
X = t-Bu	5.87 ± 1.62	2.08 ± 0.014	−1.42 ± 3.90	0.0035 ± 0.0015
X = CO$_2$Me	5.69 ± 1.41	2.07 ± 0.011	−4.16 ± 3.42	0.0030 ± 0.0036

specimens showed characteristic signals at 2θ values of 1.85° (d spacing of 4.8 nm) and 5–40° (d spacings of 1.17, 5.83 and 0.39 nm). These results suggest that the meso- and molecular-scale periodicities in the structures were similar to those of pure BPy-PMO (Fig. 1a). The other Ru(X)-BPy-PMOs (X = H, Me and t-Bu) also generated similar XRD patterns (Fig. S1–S3†). The nitrogen adsorption and desorption isotherms for the Ru(X)-BPy-PMOs were type IV and the materials were determined to have BET surface areas of 730–665 m^2 g^{-1}, pore volumes of 0.41–0.38 cm^3 g^{-1} and pore diameters of 3.8–3.5 nm (Fig. 1b, S1–S3† and Table 1). These parameters were all decreased relative to those of the original BPy-PMO following the intro-duction of the Ru complexes, meaning that the complexes were successfully generated on the internal pore surfaces. Trans-mission electron microscopy (TEM) images demonstrated that the Ru(CO$_2$Me)-BPy-PMO comprised fibrous particles with widths of several hundred nanometres (Fig. 1c). The magnified image in Fig. 1d shows one-dimensional channels running along the fibre direction with intervals of 4–5 nm. This image also confirms a lack of aggregation of the Ru metal particles during the complex formation process under these reaction conditions, with similar results apparent in the TEM images of the other Ru(X)-BPy-PMOs (X = H, Me and t-Bu).

In order to obtain information concerning the local coordi-nation structures of the Ru complexes, XAFS data were acquired from the Ru(X)-BPy-PMO specimens (Fig. S4–S7†). Ru K-edge X-ray absorption near edge structure (XANES) and EXAFS analyses suggested the successful formation of the Ru complexes on the PMO surfaces. Fig. S4 and S6† present the XANES spectra acquired from the Ru(X)-BPy-PMO samples and the homoge-neous Ru complexes. Each spectrum contains a peak at 22 144 eV and the shape and intensity of each peak are almost identical, demonstrating that the Ru(X)-BPy-PMO materials had similar coordination structures, electronic states and complex symmetries to those of the homogeneous Ru complexes. Curve fitting analyses of the Fourier transformed EXAFS data were carried out in R-space to estimate the coordination number (CN) and bond distance associated with Ru local coordination for each sample (Fig. S5 and S7†), with the results provided in Tables 2 and S1.† The CNs and bond distances for Ru–N coor-dination in the homogeneous Ru complexes were fitted to give values of 5.9–6.1 ± 1.8–2.9 and 2.07–2.08 ± 0.01–0.02 angstrom, respectively. Very similar local structures were determined for the Ru(X)-BPy-PMO products, with CN values of 5.7–6.1 ± 1.4–2.5 and bond distances of 2.07–2.08 ± 0.01 Å (Tables 2 and S1†).

UV-vis diffuse reflectance spectra generated by the Ru(X)-BPy-PMOs showed intense $\pi \rightarrow \pi^*$ absorptions at 300 nm and a characteristic absorption band in the region of 400–600 nm, assignable to dπ-to-π^* MLCT transitions (Fig. 2).[17] Ru(Me)-BPy-PMO and Ru(t-Bu)-BPy-PMO, both having electron donating groups on the X$_2$bpy moiety, showed λ_{max} values for the MLCT that were slightly blue-shifted from the 445 nm value for the Ru(H)-BPy-PMO, to 438 nm. In contrast, the MLCT band produced by the Ru(CO$_2$Me)-BPy-PMO (having electron-withdrawing ligands) was observed at 470 nm. The MLCT absorptions of the Ru(X)-BPy-PMOs were also found to be similar to those of the corresponding homogeneous Ru complexes (Fig. S8–S11†). These results indicate the successful formation of four types of Ru complexes on the PMO surfaces with local coordination states close to those of the homoge-neous Ru complexes.

Water oxidation photocatalysis by the Ru(X)-BPy-PMOs

Using a combination of IrO$_2$ as a catalyst with Ru(bpy)$_3$Cl$_2$ as the redox photosensitizer, it is possible to obtain a photocatalytic system for water oxidation via a four electron process to evolve O$_2$.[6] Photocatalytic water oxidation was thus evaluated employing IrO$_2$ loaded on the Ru-BPy-PMO materials in the presence of Na$_2$S$_2$O$_8$ as a sacrificial reagent. The latter compound served to quench the [Ru(X)-BPy-PMO]$^{2+}$ excited state (Fig. S12†). In this process, the one electron oxidized species [Ru-BPy-PMO]$^{3+}$ and SO$_4^{2-}$ were afforded as a result of the following reaction.

$$2[\text{Ru-BPy-PMO}]^{2+} + \text{S}_2\text{O}_8^{2-} + h\nu \rightarrow 2[\text{Ru-BPy-PMO}]^{3+} + 2\text{SO}_4^{2-}$$
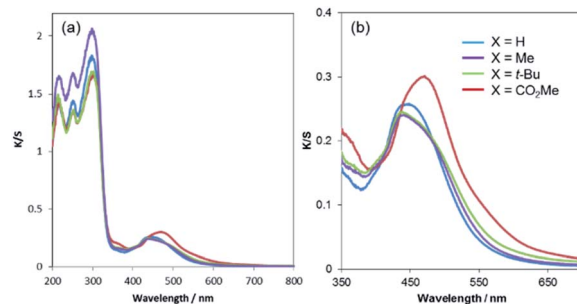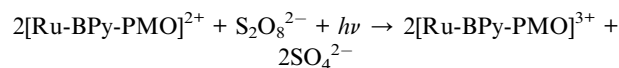

Fig. 2 UV-vis diffuse reflectance spectra of the Ru(X)-BPy-PMOs. (a) Full range spectra and (b) enlarged spectra.

The deposition of IrO_2 nanoparticles on the Ru-BPy-PMO surface was carried out *in situ via* irradiation of an aqueous $IrCl_3$ solution containing a sacrificial oxidant with visible light. TEM images of the materials show numerous aggregated particles of IrO_2 on the PMO (Fig. S13†) and the formation of these particles as a result of photoirradiation was confirmed by XAFS analyses. The XANES spectrum shows an Ir-L_{III} edge peak at 11 217 eV that can be ascribed to $Ir^{IV}O_2$ (Fig. S14†). In addition, the radial distribution function obtained from the EXAFS analysis is very similar to that of IrO_2, suggested that the original $IrCl_3$ was successfully oxidized to IrO_2. The loaded amount of Ir on the surface of PMO was carefully determined by energy-dispersive X-ray spectroscopy (EDS), which was performed using an EDS attachment to the SEM system. EDS analysis of many different areas on the Ru(CO_2Me)-BPy-PMO sample with various particle gave an atomic ratio Ir/Si of 0.05. Thus, the loading amount of Ir was calculated to be 0.324 mmol g^{-1}. IrO_2 particles forms small aggregates with diameters of 20–30 nm, confirmed by TEM and SEM images. It seems that the most effective means of dispersing the catalytic material is in the small particle form rather than as fairly large islands. Thus, the loading conditions are optimized without extensive sintering of the Ir deposit under the photocatalysis reaction. Otherwise, the low dispersion and large agglomerates of IrO_2 will occur at much higher loadings, and the IrO_2 under such conditions will have no advantages for a photocatalysis system of water oxidation.[5]

Irradiation of an aqueous suspension including Ru(H)-BPy-PMO powder generated 4.6 μmol of O_2 over a span of 22 h. This was equivalent to a TON$_{Ru}$ of 5, based on dividing the moles of product by the amount of Ru photosensitizer (Fig. 3). When using the Ru(Me)-BPy-PMO and Ru(*t*-Bu)-BPy-PMO (both of which have electron donating groups on the bpy ligands), almost no O_2 production was observed under the same conditions. In contrast, the Ru(CO_2Me)-BPy-PMO showed improved photocatalytic activity during water oxidation. Irradiation of a suspension containing Ru(CO_2Me)-BPy-PMO gave a much greater amount of oxygen (11.6 μmol over 18 h) in conjunction with a TON$_{Ru}$ of 20. This TON is higher than the values previously reported for Ru-PMO or Acd-PMO systems.[10,11]

The photocatalytic reactions using these Ru-BPy-PMO materials were found to plateau after 10–12 h, such that significant increases in oxygen production were not observed after that point. Recovered Ru(CO_2Me)-BPy-PMO showed no activity of O_2 evolution photocatalysis in the recycling use. It should be due to the decomposition of Ru complex on the surface, according to similar deactivation for a homogeneous photocatalysis system using Ru(bpy)$_3$$^{2+}$ and colloidal IrO_2, in which the amount of evolved oxygen leveled off within 1 h.[6] UV-vis diffuse reflectance spectra of Ru(CO_2Me)-BPy-PMO after photoirradiation exhibited MLCT band of Ru complex overlapped with a broad absorption in the range of 400–700 nm due to the IrO_2 nanoparticles (Fig. S19†). Normalized spectra showed a slight change in MLCT absorption band, suggesting any transformation of the coordination structure of Ru complex. Preservation of the periodic mesostructure of these materials after photocatalysis was confirmed by TEM analyses

(Fig. S13†). The observation of molecular-scale ordering in these substances indicates that the pore wall structures remained intact during the water oxidation reaction. The Ru complexes were evidently homogeneously distributed on the BPy-PMO and densely accumulated on the pore surfaces, resulting in minimal pore blockage that would otherwise hinder the diffusion of molecules in the mesochannels. It should be emphasized that all Ru complexes on the surfaces of the BPy-PMO were able to undergo electron transfer with the IrO_2 so as to promote water oxidation.

Physicochemical properties of the Ru(X)-BPy-PMOs

The photocatalytic activities of the Ru(X)-BPy-PMOs were determined by the electronic properties of the Ru complexes supported on the PMO surfaces. The presence of electron-donating or withdrawing substituents on the X_2bpy ligands changed this effect, and the π* levels of the BPy and X_2bpy ligands incorporated in the Ru(X)-BPy-PMOs were at different energies. The BPy ligands were embedded within the pore walls, such that their π* energy levels were lower compared to those of the bpy ligands. This occurred because the siloxane network (–Si–O–Si–) acted as an electron-withdrawing group with respect to the BPy moieties in the PMO framework, as indicated by previous quantum chemical calculations.[18] In the case of the X_2bpy ligands, the electron-donating groups Me and *t*-Bu shifted the energy level of the π* orbitals upwards, whereas the electron-withdrawing CO_2Me group stabilized the π* orbitals, thus lowering the energy level.[17]
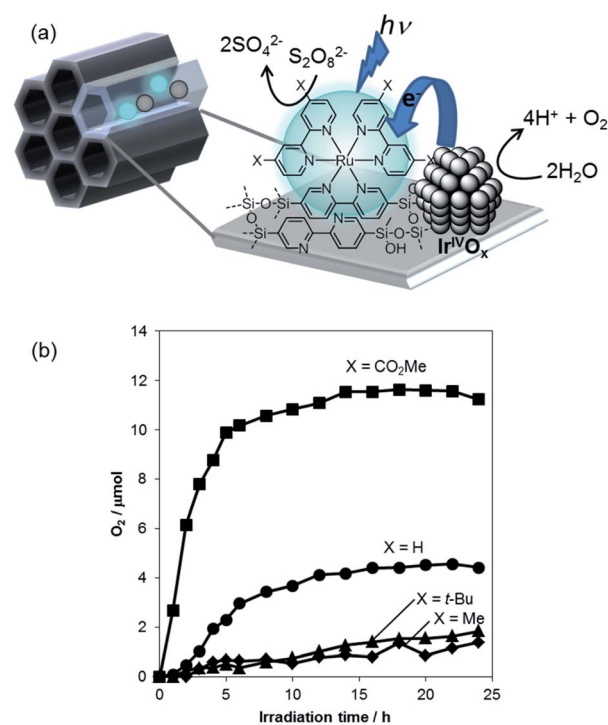

Fig. 3 (a) A schematic diagram showing the photocatalytic H_2O oxidation process. (b) Data from photocatalytic evaluations during oxygen evolution using Ru(X)-BPy-PMO (X = H, Me, *t*-Bu and CO_2Me).
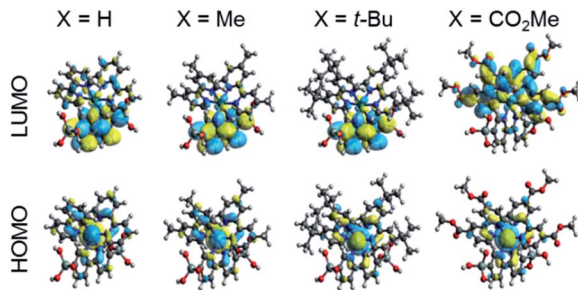
Fig. 4 Molecular orbitals of the model RuBP(X) (X = H, Me, t-Bu and CO$_2$Me).

The molecular orbitals of the Ru(X)-BPy-PMO specimens were assessed by performing quantum chemical calculations in conjunction with the model complexes Ru(sibpy)(X$_2$bpy)$_2$$^{2+}$, denoted as RuBP(X) (X = H, Me, t-Bu or CO$_2$Me) (Scheme S1†). The highest occupied molecular orbitals (HOMOs) and the lowest unoccupied molecular orbitals (LUMOs) of these RuBP(X) are presented in Fig. 4. Here, the HOMO and LUMO approximately represent the distributions of hole and excited electron in the RuBP(X) when in the lowest triplet (T$_1$) excited state, respectively (Fig. S15†). These results show that the HOMO is primarily localized on the Ru atom in all models. In contrast, the LUMO is distributed over the X$_2$bpy or sibpy ligands depending on the substituent, X. Specifically, the LUMO of RuBP(CO$_2$Me) is localized on the X$_2$bpy ligands, whereas the LUMOs of other models are spread over the sibpy ligands. These calculations suggest that, in the Ru(X)-BPy-PMOs other than Ru(CO$_2$Me)-BPy-PMO, the excited electron in the T$_1$ state is localized on the BPy group within the pore walls. In contrast, the excited electron is distributed on the X$_2$bpy ligands exposed on the pore surfaces in the case of the Ru(CO$_2$Me)-BPy-PMO. This distribution favours electron transfer to the sacrificial oxidant. Thus, these results are consistent with the experimentally-observed ordering of the photocatalytic activity.

To determine the electronic states of the Ru(X)-BPy-PMOs, the ionization potentials (IPs) of the PMO powders were obtained using photoelectron yield spectroscopy (PYS) (Fig. S16, S17 and Table S2†). The IP value for Ru(H)-BPy-PMO was

6.08 eV, whereas in the case of the Ru(Me)-BPy-PMO and Ru(t-Bu)-BPy-PMO, both of which have electron-donating groups, the IPs were slightly reduced to 5.98 and 5.90 eV. In contrast, the IP value of the Ru(CO$_2$Me)-BPy-PMO was 6.18 eV, which is attributable to the electron-withdrawing properties of the CO$_2$Me group. The IP values of the Ru(X)-BPy-PMO series were lower (that is, more positive in potential) than those of the homogeneous complexes with corresponding substituents (5.86–5.98 eV), due to the electron-withdrawing properties of the silica framework (Fig. S17†). Since the IP value (that is the HOMO level) of the Ru complex photosensitizer should be lower than the water oxidation potential (for the O$_2$/H$_2$O system), the high photocatalytic activity of Ru(CO$_2$Me)-BPy-PMO can be explained by the higher oxidizing power of the one electron-oxidized Ru complex on the PMO. The electron transfer between oxidized photosensitizer and IrO$_2$ might be rate-determining step, which are suggested by the previous study on the kinetics of electron transfer and oxygen evolution at IrO$_2$ colloids with Ru(bpy)$_3$$^{2+}$.[19]

Ru(H)-BPy-PMO suspended in Ar-saturated H$_2$O showed a characteristic phosphorescence emission band at 653 nm with a quantum yield (Φ) of 0.032 ± 0.001. This value is lower than that for homogenous Ru(bpy)$_3$Cl$_2$ in Ar-saturated H$_2$O (Φ = 0.062 ± 0.002). The Φ values for the Ru(Me)-BPy-PMO and Ru(t-Bu)-BPy-PMO (bearing electron-donating groups on the bpy ligands) were lower than that of the Ru(H)-BPy-PMO. Conversely, the Ru(CO$_2$Me)-BPy-PMO (with an electron-withdrawing group) exhibited a high Φ value of 0.042 ± 0.004. To confirm the time dependence of the phosphorescence of the Ru complexes on the PMO, time-resolved emission measurements were conducted. The decay curves monitored at 600 nm were well-fitted using a double-exponential function (Fig. S18†). On this basis, a long lifetime was assigned to the Ru complex and a short lifetime to the BPy moieties in the framework.[13] As shown in Table 3, the lifetimes decreased in the order of Ru(CO$_2$Me)-BPy-PMO > Ru(H)-BPy-PMO > Ru(Me)-BPy-PMO ≈ Ru(t-Bu)-BPy-PMO. These results are consistent with the order of the quantum yields for these same materials.

The phosphorescence of the homogeneous Ru complex Ru(bpy)$_3$Cl$_2$ was found to be quenched by oxygen molecules, resulting in a lower lifetime and quantum yield in air-saturated H$_2$O (Table 3). In contrast, almost no quenching of the

Table 3 Phosphorescence quantum yields and lifetimes of the Ru(X)-BPy-PMOs and Ru(bpy)$_3$Cl$_2$ complex

Ru(X)-BPy-PMO	Quantum yield		Lifetime/ns (fraction)	
	Ar	Air	Ar	Air
X = H	0.032 ± 0.001	0.030 ± 0.003	6.1 ± 0.2 (56%) 311 ± 2 (44%)	6.5 ± 0.3 (52%) 303 ± 2 (48%)
X = Me	0.020 ± 0.004	0.018 ± 0.004	3.9 ± 0.1 (83%) 218 ± 3 (17%)	4.0 ± 0.1 (84%) 212 ± 3 (16%)
X = t-Bu	0.019 ± 0.003	0.017 ± 0.002	4.5 ± 0.1 (82%) 208 ± 3 (18%)	4.4 ± 0.1 (83%) 209 ± 4 (17%)
X = CO$_2$Me	0.042 ± 0.004	0.041 ± 0.003	6.0 ± 0.2 (62%) 352 ± 3 (48%)	5.0 ± 0.2 (62%) 335 ± 2 (48%)
Ru(bpy)$_3$Cl$_2$	0.062 ± 0.002	0.041 ± 0.001	511 ± 11	364 ± 8

phosphorescence produced by the Ru(X)-BPy-PMOs was observed even in the presence of oxygen. Thus, these materials maintained their emission lifetimes and quantum yields. The Ru complexes on the PMO surfaces are evidently unaffected by oxygen. This is attributed to the restricted diffusion of the gas through the pores, while the homogeneous complex in the excited state is quenched by energy transfer to oxygen.

The Ru(H)-BPy-PMO, Ru(Me)-BPy-PMO and Ru(*t*-Bu)-PMO all exhibited weak emission with short lifetimes, resulting in low photocatalytic activity in the water oxidation system. In contrast, the Ru(CO_2Me)-BPy-PMO showed good photochemical properties in conjunction with its strong emission having a long lifetime. These data demonstrate that this compound is not affected by oxygen in the excited state. As demonstrated by the quantum chemical calculations (Fig. 4), an electron on a Ru atom in Ru(CO_2Me)-BPy-PMO will be excited to the X_2bpy ligands by photo-irradiation, while electrons in the Ru(X)-BPy-PMO compounds with X = H, Me or *t*-Bu will be excited to the BPy in the PMO framework. It is therefore evident that the Ru(CO_2Me)-BPy-PMO favours the interaction of the electron with the sacrificial reagent in the triplet state at the pore surfaces. These phenomena explain why Ru(CO_2Me)BPy-PMO was the most efficient photocatalyst for water oxidation.

Conclusions

A novel heterogeneous photocatalyst was constructed on a BPy-PMO surface by immobilizing tris(2,2′-bipyridine)ruthenium as a photosensitizer together with IrO_2 as a catalyst. Under visible-light irradiation, this material promoted water oxidation to generate oxygen with a high TON$_{Ru}$ value based on the amount of Ru photosensitizer. The photocatalytic activity was found to greatly depend on the photochemical properties of the Ru complex, based on the use of X_2bpy ligands having either electron-donating or withdrawing groups. These ligands therefore permitted tuning of the photochemical properties of the Ru(X)-BPy-PMO, such that the electron transfer cascade associated with photocatalysis could be optimized. The unique, highly ordered surface of PMO thus shows promise with regard to the synthesis of a new class of functional heterogeneous photocatalysts suitable for constructing artificial photosynthesis systems.

Conflicts of interest

There are no conflicts to declare.

Acknowledgements

Notes and references

1 R. Guerrero-Lemus and J. M. Martnez-Duart, in *Renewable Energies and CO₂*, Springer, London, 2013.

2 K. Hanjalic, R. van de Krol and A. Lekic, in *Sustainable Energy Technologies*, Springer, Dordrecht, 2008; Q. Li, in *Nanomaterials for Sustainable Energy*, Springer, International Publishing, 2016.

3 J. D. Blakemore, R. H. Crabtree and G. W. Brudvig, *Chem. Rev.*, 2015, **115**, 12974–13005; M. D. Kärkäs, O. Verho, E. V. Johnston and B. Åkermart, *Chem. Rev.*, 2014, **114**, 11863–12001; G. Sahara and O. Ishitani, *Inorg. Chem.*, 2015, **54**, 5096–5104; H. Li, W. Tu, Y. Zhou and Z. Zou, *Adv. Sci.*, 2016, 1500389; P. Xu, N. S. McCool and T. E. Mallouk, *Nano Today*, 2017, **14**, 42–58; V. Artero, M. Chavarot-Kerlidou and M. Fontecave, *Angew. Chem., Int. Ed.*, 2011, **50**, 7238–7266.

4 K. Kalyanasundaram and M. Grätzel, *Angew. Chem., Int. Ed. Engl.*, 1979, **18**, 701–702; E. Amouyal, *Sol. Energy Mater. Sol. Cells*, 1995, **38**, 249–276; F. Teply, *Collect. Czech. Chem. Commun.*, 2011, **76**, 859–917; L. Wang, M. Mirmohandes, A. Brown, L. Duan, F. Li, Q. Daniel, R. Lomoth, L. Sun and L. Hammarström, *Inorg. Chem.*, 2015, **54**, 2742–2751; S. Berardi, L. Francàs, S. Neudeck, S. Maji, J. Benet-Buchholz, F. Meyer and A. Llobet, *ChemSusChem*, 2015, **8**, 3688–3696.

5 A. Harriman, I. J. Pickering, J. M. Thomas and P. A. Christensen, *J. Chem. Soc., Faraday Trans. 1*, 1988, **84**, 2795–2806.

6 G. B. Saupe and T. E. Mallouk, *J. Phys. Chem. B*, 1997, **101**, 2508–2513; M. Hara and T. E. Mallouk, *Chem. Commun.*, 2000, 1903–1904; M. Hara, C. C. Waraksa, J. T. Lean, B. A. Lewis and T. E. Mallouk, *J. Phys. Chem. A*, 2000, **104**, 5275–5280; M. Hara, J. T. Lehn and T. E. Mallouk, *Chem. Mater.*, 2001, **13**, 4668–4675.

7 P. K. Ghosh, B. S. Brunschwig, M. Chou, C. Creutz and N. Sutin, *J. Am. Chem. Soc.*, 1984, **106**, 4772–4783.

8 W. J. Hunks and G. A. Ozin, *J. Mater. Chem.*, 2005, **15**, 3716–3724; F. Hoffmann, M. Cornelius, J. Morell and M. Fröba, *Angew. Chem., Int. Ed.*, 2006, **45**, 3216–3251.

9 S. Inagaki, S. Guan, Y. Fukushima, T. Ohsuna and O. Terasaki, *J. Am. Chem. Soc.*, 1999, **121**, 9611–9614; T. Asefa, M. J. MacLachlan, N. Coombs and G. A. Ozin, *Nature*, 1999, **402**, 867–871; B. J. Melde, B. T. Holland, C. F. Blanford and A. Stein, *Chem. Mater.*, 1999, **11**, 3302–3308.

10 H. Takeda, M. Ohashi, Y. Goto, T. Ohsuna, T. Tani and S. Inagaki, *Chem.–Eur. J.*, 2014, **20**, 9130–9136.

11 H. Takeda, M. Ohashi, Y. Goto, T. Ohsuna, T. Tani and S. Inagaki, *Adv. Funct. Mater.*, 2016, **26**, 5068–5077.

12 M. Waki, Y. Maegawa, K. Hara, Y. Goto, S. Shirai, Y. Yamada, N. Mizoshita, T. Tani, S. Muratsugu, M. Tada, A. Fukuoka and S. Inagaki, *J. Am. Chem. Soc.*, 2014, **136**, 4003–4011.

13 Y. Kuramochi, M. Sekine, K. Kitamura, Y. Maegawa, Y. Goto, S. Shirai, S. Inagaki and H. Ishida, *Chem.–Eur. J.*, 2017, **23**, 10301–10309; M. Waki, K.-i. Yamanaka, S. Shirai,

Y. Maegawa, Y. Goto, Y. Yamada and S. Inagaki, *Chem.–Eur. J.*, 2018, **24**, 3846–3853.

14 D. Hesek, Y. Inoue, S. R. L. Everitt, H. Ishida, M. Kunieda and M. G. B. Drew, *J. Chem. Soc., Dalton Trans.*, 1999, 3701–3709.

15 S. Rau, B. Schäfer, A. Grüßing, S. Schebesta, K. Lamm, J. Vieth, H. Görls, D. Walther, M. Rudolph, U. W. Grummt and E. Birkner, *Inorg. Chim. Acta*, 2004, **357**, 4496–4503.

16 S. A. MacFarland, F. S. Lee, K. A. W. Y. Cheng, F. L. Cozens and N. P. Schepp, *J. Am. Chem. Soc.*, 2005, **127**, 7065–7070.

17 W. F. Wacholtz, R. A. Auerbach and R. H. Schmehl, *Inorg. Chem.*, 1986, **25**, 227–234; M. Furue, K. Maruyama, T. Oguni, M. Naiki and M. Kamachi, *Inorg. Chem.*, 1992, **31**, 3792–3795; D. L. Ashford, M. K. Brennaman, R. J. Brown, S. Keinan, J. J. Concepcion, J. M. Papanikolas, J. L. Templeton and T. J. Meyer, *Inorg. Chem.*, 2015, **54**, 460–469.

18 S. Shirai, S. Iwata, Y. Maegawa, T. Tani and S. Inagaki, *J. Phys. Chem. A*, 2012, **116**, 10194–10202; S. Shirai, M. Waki, Y. Maegawa, Y. Yamada and S. Inagaki, *New J. Chem.*, 2019, **43**, 2471–2478.

19 N. D. Morris, M. Suzuki and T. E. Mallouk, *J. Phys. Chem. A*, 2004, **108**, 9115–9119.